Marchenko imaging: Imaging with primaries, internal multiples, and free-surface multiples

Satyan Singh[1], Roel Snieder[1], Jyoti Behura[2], Joost van der Neut[3],
Kees Wapenaar[3], and Evert Slob[3]

ABSTRACT

Recent work on retrieving the Green's function with the Marchenko equation shows how these functions for a virtual source in the subsurface can be obtained from reflection data. The response to the virtual source is the Green's function from the location of the virtual source to the surface. The Green's function is retrieved using only the reflection response of the medium and an estimate of the first arrival at the surface from the virtual source. Current techniques, however, only include primaries and internal multiples. Therefore, all surface-related multiples must be removed from the reflection response prior to Green's function retrieval. We have extended the Marchenko equation to retrieve the Green's function that includes primaries, internal multiples, and free-surface multiples. In other words, we have retrieved the Green's function in the presence of a free surface. The information needed for the retrieval is the same as the current techniques, with the only difference being that the reflection response now also includes free-surface multiples. The inclusion of these multiples makes it possible to include them in the imaging operator, and it obviates the need for surface-related multiple elimination. This type of imaging with Green's functions is called *Marchenko imaging*.

INTRODUCTION

To focus a wavefield at a point in a medium only requires surface reflection data and an estimate of the first-arriving wave at the surface from a point source at the focusing location (Broggini et al., 2012; Broggini and Snieder, 2012; Wapenaar et al., 2013a). Unlike in seismic interferometry (Bakulin and Calvert, 2006; Wapenaar and Fokkema, 2006), no receiver is required at the desired focusing location, i.e., the virtual source location and single-sided illumination suffices. Significantly, the detailed medium parameters need not be known to focus the wavefield as opposed to the time-reversal method, which requires the knowledge of detailed medium parameters and enclosing boundaries for correct focusing. However, the traveltime of the direct arrival of the virtual source to the surface is required for Green's function retrieval. To obtain an estimate of this traveltime, one only needs a macromodel of the velocity.

The focusing scheme of Broggini et al. (2012), Broggini and Snieder (2012), and Wapenaar et al. (2013a) is an extension of the algorithm of Rose (2002a, 2002b), who shows an iterative scheme that solves the Marchenko equation for wavefield focusing in 1D. The focused events in the wavefield for the virtual source consist of primaries and internal multiples (Wapenaar et al., 2013a) but not free-surface multiples. Importantly, Rose (2002a, 2002b) derives the focusing method for single-sided illumination with sources and receivers on one side of the medium, similar to current geophysical acquisition methods.

Wapenaar et al. (2011) illustrate imaging with the Green's function in 1D and also discuss how to image in multidimensions (2D and 3D). Similarly, Behura et al. (2012) introduce a correlation-imaging algorithm based on the Green's function retrieval scheme that images not only primaries but also internal multiples. Broggini et al. (2014) extend the work of Behura et al. (2012) by using multidimensional deconvolution (MDD) as the imaging condition in place of conventional crosscorrelation or deconvolution, which further reduces the artifacts. Central in these methods is the retrieval of the Green's function from the acquisition surface to any point in the

medium. This Green's function is essentially a redatuming or downward continuation operator. Because this Green's function includes primaries and internal multiples, we expect improved subsurface images compared with using primaries alone.

We summarize our work in Figure 1. In this paper, any variable with a subscript zero (e.g., R_0) indicates that no free surface is present. As shown in Figure 1, prior to the algorithm of Broggini et al. (2012), one must remove the free-surface multiples from the reflection response of the medium (solid upgoing arrow) to retrieve the Green's function. The removal of the free-surface multiples can be achieved by surface-related multiple elimination (SRME) (Verschuur et al., 1992). In our study, we modify the earlier focusing algorithms (Rose, 2002a; Broggini et al., 2012; Wapenaar et al., 2013a) to focus not only primaries and internal multiples but also the free-surface multiples; this is labeled "Our work" in Figure 1. We achieve such focusing using the reflection response R in the presence of a free surface and an estimate of the first arrival from the focus location to the surface. Notably, our proposed Green's function retrieval scheme obviates the need for SRME (see Figure 1) to construct the Green's function.

The free surface is the strongest reflector in the system; therefore, in general, the free-surface multiples are stronger than internal multiples. In addition, free-surface multiples can be used to provide better illumination, higher fold, and better vertical resolution of the subsurface (Schuster et al., 2003; Jiang et al., 2007; Muijs et al., 2007a, 2007b). For these reasons, by retrieving the Green's function, which includes primaries and all multiples (including free-surface multiples), and using the imaging condition proposed by Behura et al. (2012) and by Broggini et al. (2014), we expect better imaging of the subsurface.

THEORY

In this section, we derive the main equations for the retrieval of the Green's function in the presence of a free surface, with the detailed derivations in Appendix A. We first summarize the existing theory that this paper is building on.

The theory of focusing the wavefield without a free surface, i.e., retrieving the Green's function G_0 from R_0, is covered by Rose
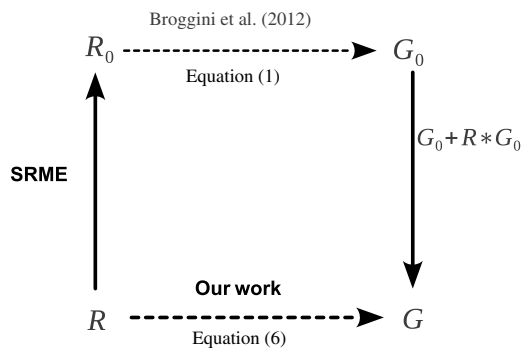
Figure 1. Overview of the methods to focus the wavefield using an iterative approach. The R denotes reflected waves recorded at the surface in the presence of a free surface, and R_0 is the reflection response for a medium without a free surface. The G is the Green's function at the surface for a virtual source located at a point in the medium in the presence of a free surface, and G_0 is the Green's function in the absence of a free surface. The two dashed arrows indicate separate iterative schemes.

(2002a), Broggini et al. (2012), and Wapenaar et al. (2013a). As summarized in Figure 1, we have to remove the free-surface multiples from the reflection response R (for instance, by SRME) to get R_0 and then compute G_0, the Green's function in the absence of the free surface.

Wapenaar et al. (2004) show that we can relate the transmission operators for media with and without the free surface. Similarly, we can retrieve G (the Green's function in the presence of the free surface) from G_0 in the frequency domain with the expression

$$G(\mathbf{x_i'}, \mathbf{x_0}, \omega) = G_0(\mathbf{x_i'}, \mathbf{x_0}, \omega)$$
$$- \int_{\partial D_0} G_0(\mathbf{x_i'}, \mathbf{x}, \omega) R(\mathbf{x}, \mathbf{x_0}, \omega) d\mathbf{x}, \quad (1)$$

where ∂D_0 is the acquisition surface, $\mathbf{x_0}$ and $\mathbf{x_i'}$ are spatial positions along ∂D_0 and ∂D_i (an arbitrary depth level, below ∂D_0), and R is the reflection response for a downgoing incident wavefield at ∂D_0. The arbitrary depth levels are defined in the same way as in the work of Wapenaar et al. (2004). In our case, we replace the transmission responses (in equation 22 of Wapenaar et al., 2004) with the corresponding Green's functions G or G_0 because the Green's function is the total transmitted wavefield from the focusing point to the surface. Note that this approach, $R \rightarrow R_0 \rightarrow G_0 \rightarrow G$, follows the tortuous path shown in Figure 1. We can, however, retrieve the Green's function in the presence of the free surface directly from the measured reflection data $R \rightarrow G$ (Figure 1, black dashed arrow). Therefore, $R \rightarrow G$ avoids SRME and the retrieval of G_0. We generalize the formulation of Wapenaar et al. (2013a) ($R_0 \rightarrow G_0$) to include free-surface multiples ($R \rightarrow G$); the detailed mathematics of this retrieval is documented in Appendix A. The reflections from the free surface are included in the focusing scheme, similar to the treatment by Wapenaar et al. (2004) of free-surface multiples.

We define our spatial coordinates by their horizontal and depth components, for instance, $\mathbf{x_0} = (\mathbf{x_H}, x_{3,0})$, where $\mathbf{x_H}$ denotes the horizontal coordinates (x_1, x_2) at a depth $x_{3,0}$. We define solutions of the wave equation that focus at a point in a medium, and we refer to these as the focusing functions f_1 and f_2. The f_1 function involves waves that focus at $\mathbf{x_i'}$ at a defined depth level (∂D_i) for incoming and outgoing waves at the acquisition surface (∂D_0) at $\mathbf{x_0}$ (Figure 2a). The function f_2 is a solution for waves that focus just above ∂D_0 at $\mathbf{x_0''}$ for incoming and outgoing waves at ∂D_i (Figure 2b).

The focusing functions are auxiliary wavefields, which exist in a reference medium that has the same material properties as the actual inhomogeneous medium between ∂D_0 and ∂D_i and that is homogeneous above ∂D_0 and reflection-free below ∂D_i (Slob et al., 2014). Therefore, the boundary conditions on ∂D_0 and ∂D_i in the reference medium, where the focusing function exists, are reflection free.

Note that this boundary condition need not be the same as the actual medium. The focusing functions can be separated into up- and downgoing waves; the first focusing function in the frequency domain reads

$$f_1(\mathbf{x}, \mathbf{x_i'}, \omega) = f_1^+(\mathbf{x}, \mathbf{x_i'}, \omega) + f_1^-(\mathbf{x}, \mathbf{x_i'}, \omega), \quad (2)$$

whereas the second focusing function reads

$$f_2(\mathbf{x}, \mathbf{x_0''}, \omega) = f_2^+(\mathbf{x}, \mathbf{x_0''}, \omega) + f_2^-(\mathbf{x}, \mathbf{x_0''}, \omega). \quad (3)$$

The figure contains:

Broggini et al. (2012)

R_0 - - - - - - - - - - - → G_0
Equation (1)

$G_0 + R * G_0$

SRME

Our work

R - - - - - - - - - - - → G
Equation (6)

In this paper, the superscript $+$ refers to downgoing waves and $-$ refers to upgoing waves at the observation point $\mathbf{x}$.

Table 1 and Figure 2a show the one-way wavefields for the f_1 function at the depth levels ∂D_0 and ∂D_i, which we define in wave state A. We call these waves one way because locally these fields are strictly up- or downgoing at the observation point; however, their coda will include the up- and downgoing waves.

The focusing function $f_1^+(\mathbf{x}, \mathbf{x_i'}, t)$ is shaped such that $f_1(\mathbf{x}, \mathbf{x_i'}, t)$ focuses at $\mathbf{x_i'}$ at $t = 0$. At the focusing depth level ∂D_i of f_1, we define $f_1(\mathbf{x}, \mathbf{x_i'}, t)$ as $\delta(\mathbf{x_H} - \mathbf{x_H'})\delta(t)$, a 2D and 1D Dirac delta function in space and time, respectively (see Figure 2b and Table 1). Below the focusing depth level, $f_1(\mathbf{x}, \mathbf{x_i'}, t)$ continues to diverge as a downgoing field $f_1^+(\mathbf{x}, \mathbf{x_i'}, t)$ into the reflection-free reference half-space.

Similarly, Table 2 and Figure 2b show the one-way wavefields for the f_2 function at the depth levels ∂D_0 and ∂D_i.

In this case, $f_2^-(\mathbf{x}, \mathbf{x_0''}, t)$ is shaped such that the function $f_2(\mathbf{x}, \mathbf{x_0''}, t)$ focuses at $\mathbf{x_0''}$ at $t = 0$. At the focusing depth level ∂D_0 of f_2, we define $f_2(\mathbf{x}, \mathbf{x_0''}, t)$ as $\delta(\mathbf{x_H} - \mathbf{x_H''})\delta(t)$ (see Figure 2b and Table 2). After focusing, $f_2(\mathbf{x}, \mathbf{x_0''}, t)$ continues to diverge as an upgoing field $f_2^-(\mathbf{x}, \mathbf{x_0''}, t)$ into the homogeneous upper half-space.

The focusing functions are independent of the surface boundary condition of the actual medium because these functions reside only in the reference medium. If the media were homogeneous, the focusing function f_2 would consist of the time-reversed direct wave between the focal point and ∂D_i. However, in an inhomogeneous medium, the focusing function f_2 consists of the time-reversed direct wave and the coda M following the time-reversed direct wave. The coda M consists of the scattered waves that result when the time-reversed direct wave transmits through the medium to the focus point.
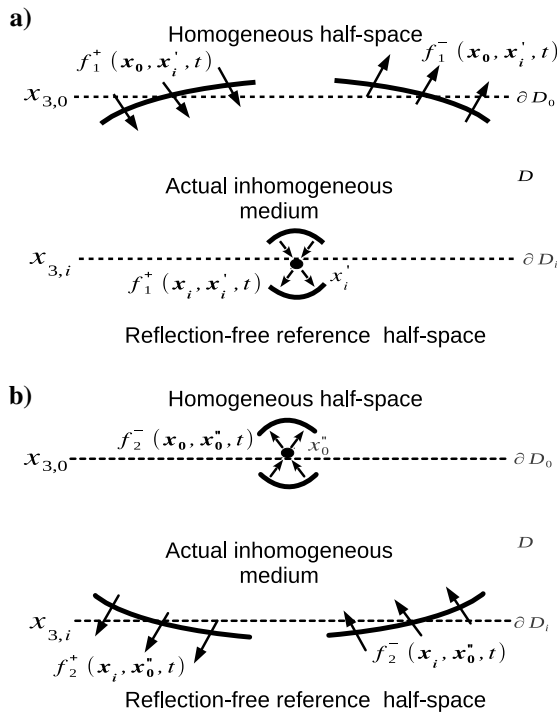
In the frequency domain, the focusing function f_2 is related to the Green's function G_0 of the actual inhomogeneous medium without a free surface by (Wapenaar et al., 2013a)

$$G_0(\mathbf{x_i'}, \mathbf{x_0''}, \omega) = f_2(\mathbf{x_i'}, \mathbf{x_0''}, \omega)^*$$
$$+ \int_{\partial D_0} f_2(\mathbf{x_i'}, \mathbf{x_0}, \omega) R_0(\mathbf{x_0}, \mathbf{x_0''}, \omega) d\mathbf{x_0}, \quad (4)$$

where $*$ represents the complex conjugate. In a situation without the free surface, we ignore the downward-reflected waves at the acquisition level, i.e., the free surface multiples. In the actual inhomogeneous medium, in the presence of a free surface, we account for the waves reflecting from the free surface (details are given in Appendix A, as shown in equation A-5). For this situation, the one-way wavefields are shown in Table 3 and Figure 3. We define wave state B as the acoustic state with the wavefields of the actual medium (Wapenaar et al., 2013a).

We can use the one-way reciprocity theorems of the convolution and correlation type for flux-normalized one-way wavefields (Wapenaar and Grimbergen, 1996):

Table 1. One-way wavefields of the focusing function f_1 at the acquisition surface ∂D_0 and the level where f_1 focuses ∂D_i. The symbol $p_A^{\pm}$ represents one-way wavefields in the frequency domain, at arbitrary depth levels in the reference medium (see Figure 2a).

On ∂D_0:	$p_A^+ = f_1^+(\mathbf{x_0}, \mathbf{x_i'}, \omega)$
	$p_A^- = f_1^-(\mathbf{x_0}, \mathbf{x_i'}, \omega)$
On ∂D_i:	$p_A^+ = f_1^+(\mathbf{x_i}, \mathbf{x_i'}, \omega) = \delta(\mathbf{x_H} - \mathbf{x_H'})$
	$p_A^- = f_1^-(\mathbf{x_i}, \mathbf{x_i'}, \omega) = 0$

Table 2. One-way wavefields of the focusing function f_2 at the depth level ∂D_0 and ∂D_i. The symbol $p_A^{\pm}$ represents one-way wavefields in the frequency domain, at arbitrary depth levels in the reference medium (see Figure 2b).

On ∂D_0:	$p_A^+ = f_2^+(\mathbf{x_0}, \mathbf{x_0''}, \omega) = 0$
	$p_A^- = f_2^-(\mathbf{x_0}, \mathbf{x_0''}, \omega) = \delta(\mathbf{x_H} - \mathbf{x_H''})$
On ∂D_i:	$p_A^+ = f_2^+(\mathbf{x_i}, \mathbf{x_0''}, \omega)$
	$p_A^- = f_2^-(\mathbf{x_i}, \mathbf{x_0''}, \omega)$

Table 3. One-way wavefields in the actual inhomogeneous medium in the presence of a free surface at the depth level ∂D_0 and ∂D_i. The symbol $p_B^{\pm}$ represents one-way wavefields at arbitrary depth levels in the inhomogeneous medium, whereas r is the reflection coefficient of the free surface (see Figure 3).

On ∂D_0:	$p_B^+ = G^+(\mathbf{x_0}, \mathbf{x_0''}, \omega) = \delta(\mathbf{x_H} - \mathbf{x_H''}) + rR(\mathbf{x_0}, \mathbf{x_0''}, \omega)$
	$p_B^- = G^-(\mathbf{x_0}, \mathbf{x_0''}, \omega) = R(\mathbf{x_0}, \mathbf{x_0''}, \omega)$
On ∂D_i:	$p_B^+ = G^+(\mathbf{x_i}, \mathbf{x_0''}, \omega)$
	$p_B^- = G^-(\mathbf{x_i}, \mathbf{x_0''}, \omega)$

Figure 2. (a) Focusing function f_1 that focuses at $\mathbf{x_i'}$ and (b) focusing function f_2 that focuses at $\mathbf{x_0''}$.

$$\int_{\partial D_0} [p_A^+ p_B^- - p_A^- p_B^+] d\mathbf{x_0} = \int_{\partial D_i} [p_A^+ p_B^- - p_A^- p_B^+] d\mathbf{x_i},$$

$$\int_{\partial D_0} [(p_A^+)^* p_B^+ - (p_A^-)^* p_B^-] d\mathbf{x_0} = \int_{\partial D_i} [(p_A^+)^* p_B^+ - (p_A^-)^* p_B^-] d\mathbf{x_i},$$

$$\text{(5)}$$

respectively, to relate the one-way wavefields between the two focusing functions (f_1 and f_2) and the one-way wavefields between the focusing functions and the actual medium. Here, $p_A^\pm$ and $p_B^\pm$ are the one-way wavefields of the focusing functions and the actual medium, respectively, in the frequency domain. As shown in Appendix A, the corresponding two-way Green's function in the presence of the free surface is related to the focusing function f_2 by

$$G(\mathbf{x_i'}, \mathbf{x_0''}, \omega) = f_2(\mathbf{x_i'}, \mathbf{x_0''}, \omega)^*$$
$$+ \int_{\partial D_0} f_2(\mathbf{x_i'}, \mathbf{x_0}, \omega) R(\mathbf{x_0}, \mathbf{x_0''}, \omega) d\mathbf{x_0}$$
$$+ r \int_{\partial D_0} f_2(\mathbf{x_i'}, \mathbf{x_0}, \omega)^* R(\mathbf{x_0}, \mathbf{x_0''}, \omega) d\mathbf{x_0}, \quad \text{(6)}$$

where, for simplicity, we assume that the reflection coefficient of the free surface satisfies $r = -1$. The two-way Green's function is defined as the superposition of the down- and upgoing fields, according to

$$G(\mathbf{x}, \mathbf{x_0''}, \omega) = G^+(\mathbf{x}, \mathbf{x_0''}, \omega) + G^-(\mathbf{x}, \mathbf{x_0''}, \omega). \quad \text{(7)}$$

Using reciprocity, the Green's functions on the left side of equations 4 and 6 can be interpreted as the response to a virtual source at $\mathbf{x_i'}$ for the situation without and with a free surface, respectively. To yield equations 4 and 6, we use the one-way reciprocity relations (details are given in Appendix A for the retrieval of G, equation A-5). Note that the upgoing Green's function G^- in the actual inhomogeneous medium at ∂D_0 is the reflection response R for a downward-radiating source at ∂D_0.

Equation 6 differs from equation 4 in two ways: First, the last term on the right side of equation 6 accounts for the waves that are reflected off the free surface. Second, equation 6 contains
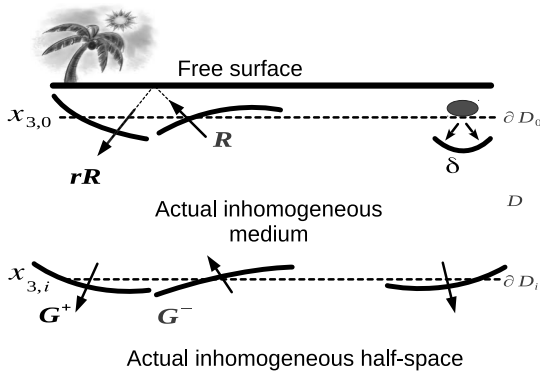

Figure 3. One-way Green's functions in the actual inhomogeneous medium in the presence of a free surface at the acquisition surface ∂D_0 and the arbitrary surface ∂D_i. These are the quantities that are used in the reciprocity theorems. The tree indicates the presence of the free surface.

the reflection response R for a medium with a free surface, whereas expression 4 contains the reflection response R_0 for a medium without a free surface.

Similar to our treatment of the focusing function f_2, we can define another focusing function g_2, such that

$$g_2(\mathbf{x}, \mathbf{x_0''}, \omega) = f_2^+(\mathbf{x}, \mathbf{x_0''}, \omega) - f_2^-(\mathbf{x}, \mathbf{x_0''}, \omega). \quad \text{(8)}$$

We use g_2 to obtain a difference Green's function $\tilde{G}$, which is similar to expression 6:

$$\tilde{G}(\mathbf{x_i'}, \mathbf{x_0''}, \omega) = -g_2(\mathbf{x_i'}, \mathbf{x_0''}, \omega)^*$$
$$+ \int_{\partial D_0} g_2(\mathbf{x_i'}, \mathbf{x_0}, \omega) R(\mathbf{x_0}, \mathbf{x_0''}, \omega) d\mathbf{x_0}$$
$$- r \int_{\partial D_0} g_2(\mathbf{x_i'}, \mathbf{x_0}, \omega)^* R(\mathbf{x_0}, \mathbf{x_0''}, \omega) d\mathbf{x_0}. \quad \text{(9)}$$

We call $\tilde{G}$ the *difference Green's function* because

$$\tilde{G}(\mathbf{x_i'}, \mathbf{x_0''}, \omega) = G^+(\mathbf{x_i'}, \mathbf{x_0''}, \omega) - G^-(\mathbf{x_i'}, \mathbf{x_0''}, \omega), \quad \text{(10)}$$

and it is used to obtain the up- and downgoing Green's functions by combining it with G in equation 7.

To yield the upgoing Green's function, we subtract equations 7 and 10:

$$G^-(\mathbf{x_i'}, \mathbf{x_0''}, \omega) = \frac{1}{2}[G(\mathbf{x_i'}, \mathbf{x_0''}, \omega) - \tilde{G}(\mathbf{x_i'}, \mathbf{x_0''}, \omega)]. \quad \text{(11)}$$

Similarly, we obtain the downgoing Green's function by adding equations 6 and 10

$$G^+(\mathbf{x_i'}, \mathbf{x_0''}, \omega) = \frac{1}{2}[G(\mathbf{x_i'}, \mathbf{x_0''}, \omega) + \tilde{G}(\mathbf{x_i'}, \mathbf{x_0''}, \omega)]. \quad \text{(12)}$$

These up- and downgoing (G^- and G^+) Green's functions at the focal point are used for imaging (Marchenko imaging) and include primaries and all multiples. Up- and downgoing Green's functions have been used for imaging the subsurface (Wapenaar et al., 2011; Behura et al., 2012; Broggini et al., 2012, 2014). However, their Green's functions contain only primaries and internal multiples. In this paper, the up- and downgoing Green's functions also include free-surface multiples.

The use of up- and downgoing wavefields for imaging is not a new principle. Claerbout (1971), Wapenaar et al. (2000), and Amundsen (2001) show that one can get the reflection response below an arbitrary depth level once the up- and downgoing wavefields are available. The governing equation that relates the up- and downgoing Green's function is

$$G^-(\mathbf{x_i'}, \mathbf{x_0''}, t)$$
$$= \int_{\partial D_i} d\mathbf{x_i} \int_{-\infty}^{\infty} G^+(\mathbf{x_i}, \mathbf{x_0''}, t - t') R_0(\mathbf{x_i'}, \mathbf{x_i}, t') dt', \quad \text{(13)}$$

where ∂D_i is an arbitrary depth level and R_0 is the reflection response of the medium below ∂D_i. In addition, R_0 at ∂D_i contains no reflections from above this depth level. We can think of R_0 as the reflection response of a truncated medium, where the truncated

medium is the same as the true medium below ∂D_i and reflection free above. Equation 13 states that G^- is represented by the convolution of G^+ with R_0 and integration along all source positions $\mathbf{x}'$ of R_0.

We solve for R_0 by MDD (Van der Neut et al., 2011) because the time integral is a convolution. The subsurface image is subsequently obtained by taking the zero lag of R_0, i.e., taking $t = 0$ at each depth level in the model and at zero offset, $\mathbf{x_i} = \mathbf{x_i'}$ (for each ∂D_i); this is called the *zero-offset imaging condition*. Alternatively, once we obtain R_0 at an arbitrary ∂D_i, we can also apply a standard imaging procedure, for instance, downward continuation, to image below ∂D_i. This is because R_0 is the reflection response of the truncated medium below ∂D_i for sources and receivers at ∂D_i.

NUMERICAL EXAMPLES

We use three numerical examples that show the retrieval of the Green's functions and imaging using the associated Green's functions.

We first consider a 1D model that has a high impedance layer generic to salt models as shown in Figure 4. A receiver at the surface records the reflected waves. To retrieve the Green's function in 1D, one needs the traveltime of the first arriving wave from the virtual source to the surface. The traveltime of the first arriving wave is used to temporally separate the Green's function from the focusing solution f_2 in the time-domain representation of equation 6. To obtain the focusing function f_2, we evaluate expression 6 for a time earlier than the first arriving wave and setting the left side of equation 6 to zero. The remaining expression is an equation for f_2, which is solved iteratively (details are given in Appendix A, equations A-6–A-10).

Once the focusing solution has been found (see Figure 5), it is substituted in equation 6 to retrieve the Green's function (for this example, the Green's function is the response to the virtual source at a depth of 2.75 km, [dot in Figure 4], recorded at the surface; Figure 6). This Green's function G, arbitrarily scaled to its maximum amplitude (see Figure 6), is the response at the surface ∂D_0 to the virtual source.

We also model the Green's function using finite differences to verify that the Green's function retrieved from our algorithm is accurate, and we superimposed this result on Figure 6. The vertical scale of Figure 6 is enlarged to better illustrate the model and retrieved Green's function. For this reason, the first arrival at time
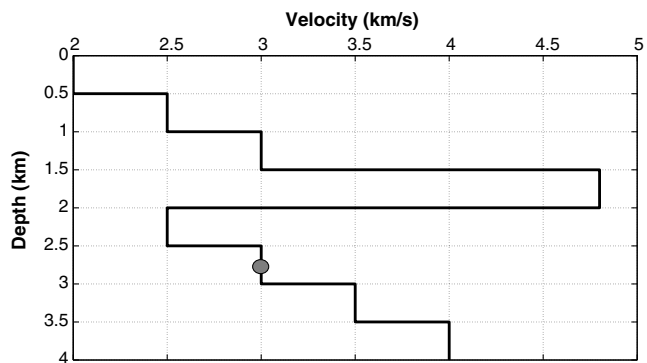
1.0 s is clipped. The difference between the modeled and the retrieved Green's function is negligible relative to the average amplitude of the Green's function, as seen in Figure 6. The arrivals caused by the free surface are shown in Figure 7 compared with the arrivals in the absence of a free surface.

The corresponding image of the model in Figure 4 shown in Figure 8 illustrates the correct location of the reflectors, as well as the correct scaled reflection coefficient. In 1D, the image we obtain is the deconvolution of the up- and downgoing Green's function for $t = 0$ at each image point (Claerbout, 1985). There are some anomalous amplitudes in the Marchenko image (especially at approximately 200 m), but they are small compared with the actual reflectors' amplitude and are attributed to the deconvolution imaging condition.

The model for the next example is taken from Weglein and Dragoset (2007), where the second primary event cancels with
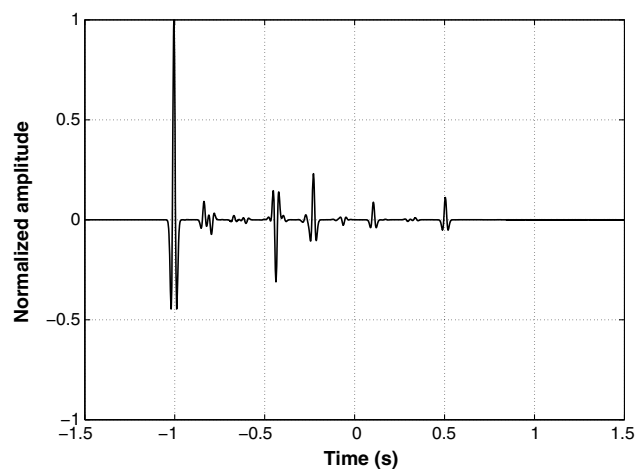

Figure 5. Focusing function f_2 at depth 2.75 km for the velocity model in Figure 4.
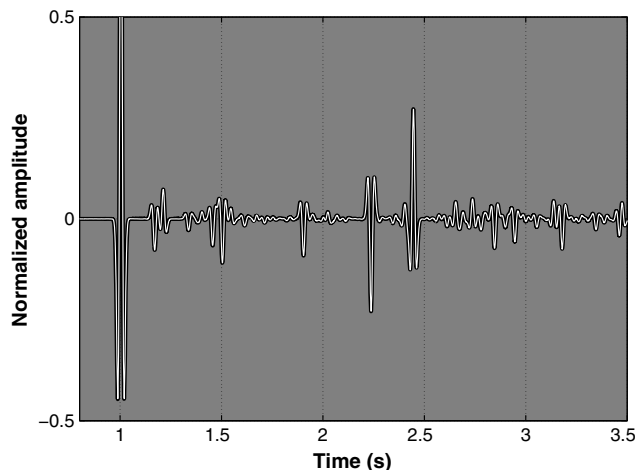

Figure 6. Retrieved Green's function (normalized by maximum amplitude) G from a depth of 2.75 km to the surface (white). The modeled Green's function is displayed (in black) in the background. The Green's functions are associated to the model in Figure 4.

Figure 4. Velocity model with high impedance layer at 1.5 km; the dot is the position of the virtual source.

the free-surface multiple from the first reflector. We demonstrate with this numerical example the retrieval of the Green's function (as well as its associated up- and downgoing Green's function)
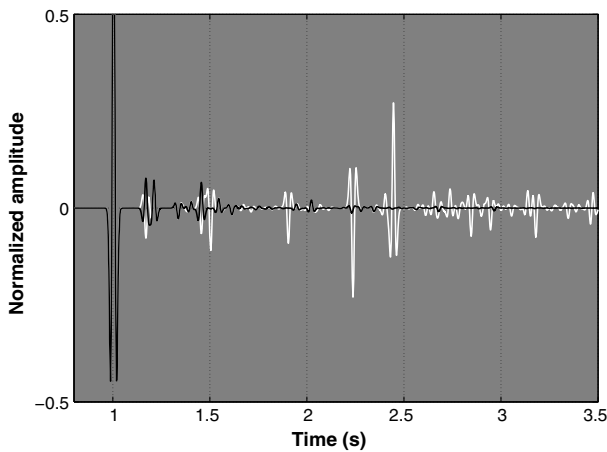

Figure 7. Impact of the free surface. The black line shows the Green's function in a medium without a free surface G_0, and the white line is the difference between G and G_0; therefore, the white line shows events that are caused by the presence of the free surface.
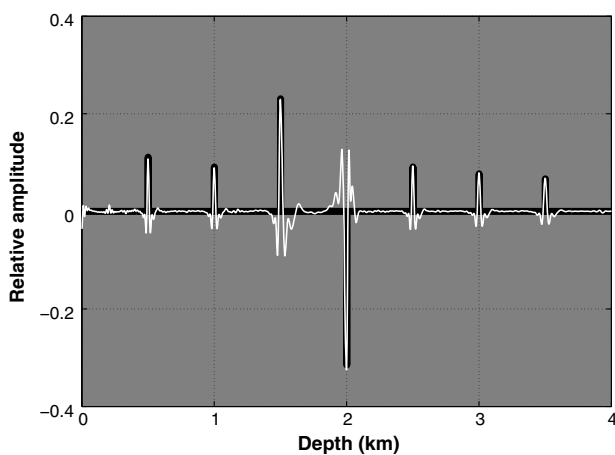

Figure 8. Marchenko imaging of Figure 4 in white, with the true reflectivity (in black) in the background.
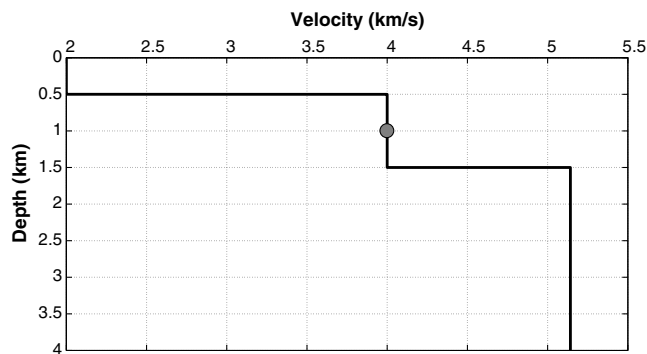
Figure 9. Simple velocity model, where the dot indicates the position of one virtual source at depth 1000 m.

at depth 1000 m for the model shown in Figure 9. Figure 10 illustrates some of the reflected events corresponding to this model. The associated reflected waves at the acquisition level, shown in Figure 11, are recorded 5 m below the free surface. As is shown in Figures 11 and 10, the second primary event P_2 is canceled by the free-surface multiple F_1 at 1.0 s, and the other events (internal multiples and free surface multiples) interfere destructively with each other at later times.

The Green's function for a source at depth 1000 m is shown in Figure 12. The corresponding up- and downgoing Green's function
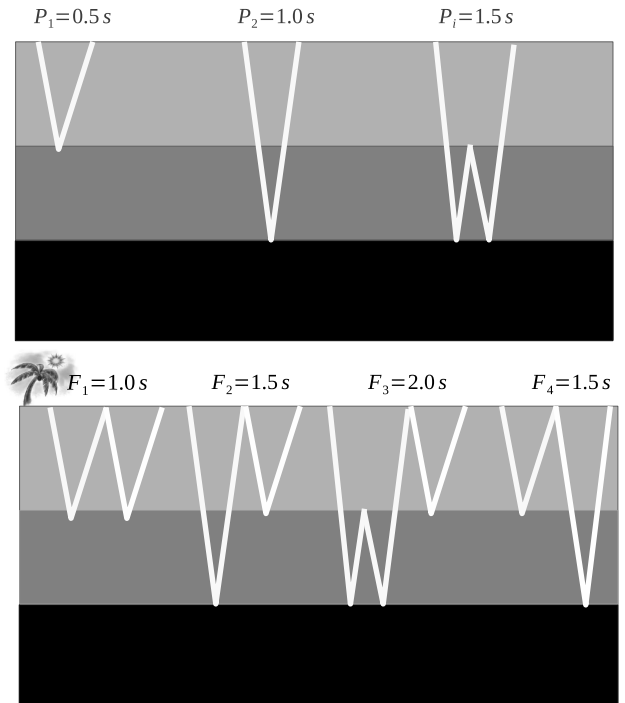

Figure 10. Sketch of some events that occur in the velocity model in Figure 9.
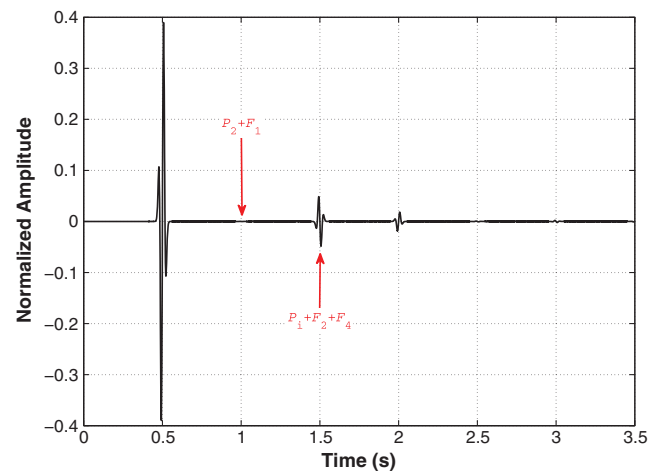

Figure 11. Reflection response with the direct waves removed (the events are scaled by the direct wave magnitude); the labels are referenced to in Figure 10.

at depth 1000 m is illustrated in Figures 13 and 14, respectively. The computed traveltimes for this simple model of the up- and down-going Green's function in Figure 15 correspond to the traveltimes of the events in the retrieved up- and downgoing Green's functions, hence confirming our decomposition of the Green's function into its associated up- and downgoing wavefields.

Figure 12 has an event at 0.6 s, which is the reflection of the virtual source field from the second layer recorded at the surface. Hence, the Green's function retrieval algorithm correctly detects the missing reflector in the recorded waves. In the 1D model considered here, equation 13, reduces to the deconvolution of the upgoing Green's function with the downgoing Green's function at every point in the velocity model yielding the correct positioning of the reflectors (see Figure 16), as well as the correct scaled reflection coefficient. Furthermore, the image is free of artifacts originating from surface-related and internal multiples. Importantly, the differ-

ence between the analysis of Weglein and Dragoset (2007) and our work is that they remove the multiples at the surface, whereas we derive the Green's function for a virtual source in the subsurface and, subsequently, a multiple-free image.

DISCUSSION

The new feature of our Green's function retrieval scheme compared with the earlier presented schemes is that we include the free-surface multiples in our Green's function. Hence, we do not need to remove the free-surface multiples from our reflection response. For our 1D numerical examples, we can identify the events that are caused by the presence of the free surface (the black line in Figure 7) by computing the difference of G and G_0.

The arrivals that are caused by the free surface (black line in Figure 7) have higher amplitude and greater waveform complexity
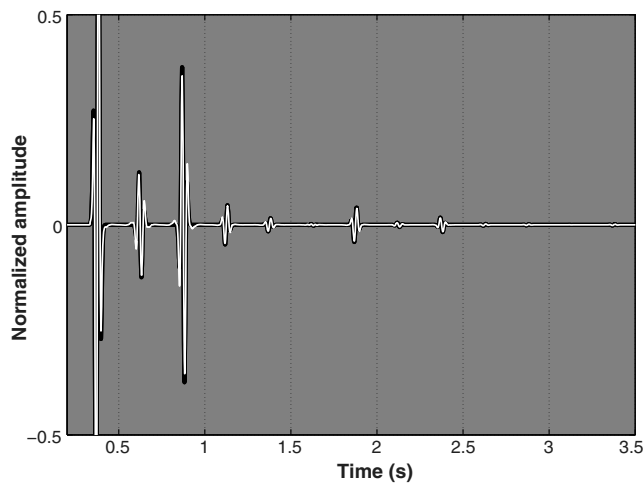

Figure 12. Green's function with virtual source at depth 1000 m and recording at the surface. The black thicker line is the modeled Green's function; superimposed on it is the retrieved Green's function. The plot limits are chosen between 0.5 and −0.5 normalized amplitude to better visualize the smaller amplitude events.

Figure 14. The Green's function for downgoing waves at the virtual source location (1000 m) and recording at the surface for the velocity in model in Figure 9.
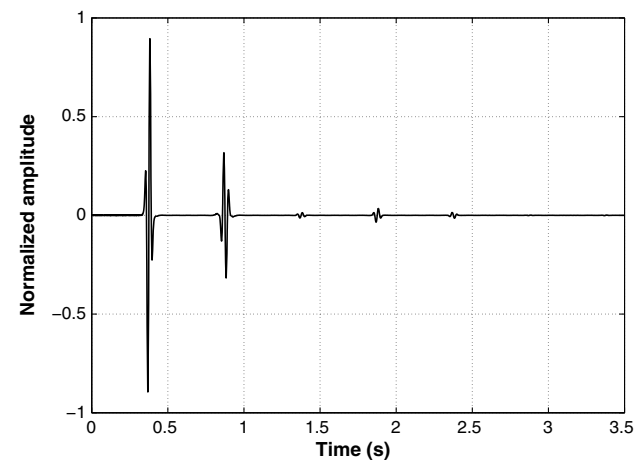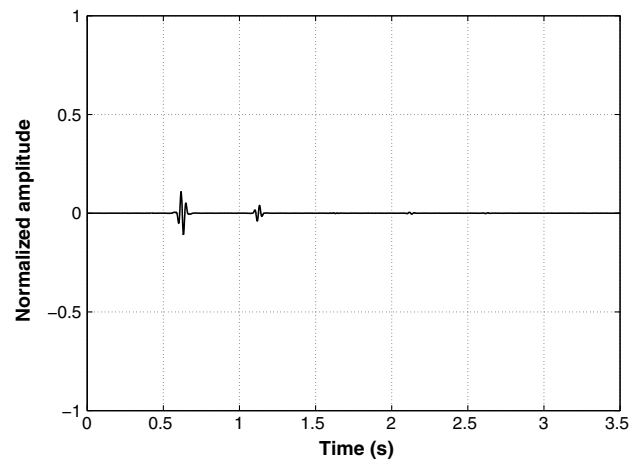

Figure 13. The Green's function for upgoing waves at the virtual source location (1000 m) and recording at the surface for the velocity in model in Figure 9.
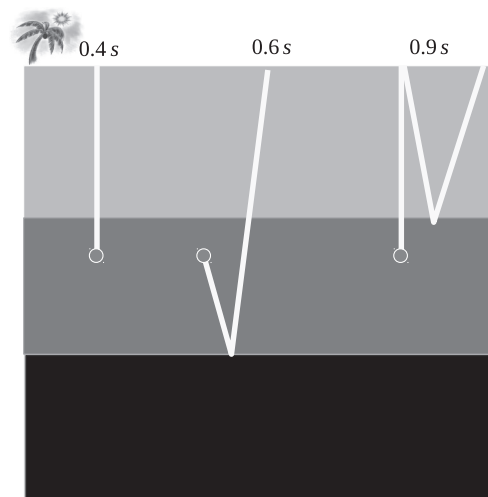

Figure 15. Sketch of some events that are present in the Green's function from the virtual source (gray dot) at 1000 m and recorded at the surface for the velocity in model in Figure 9.
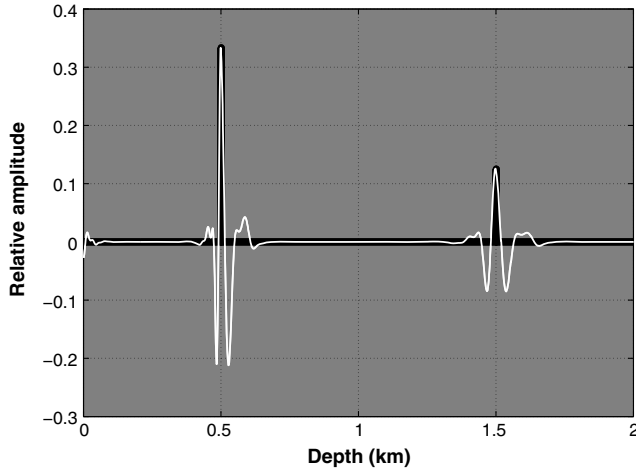
Figure 16. Image of the velocity model (Figure 9) after Marchenko imaging with the reflectivity overlain (in black).

compared with the events in the response without a free surface G_0 (white line in 7). This supports our conjecture that using the additional events and energy that free-surface reflections provide can benefit imaging of the subsurface, i.e., imaging using G rather than G_0.

In our scheme to retrieve the Green's function, we require that the wavelet is removed from the reflection response (which can be done by deconvolution). In addition, we assume that the reflection response is due to a downgoing source. However, in the marine case, the source is generally placed a few meters below the surface; therefore, there is not only a downgoing component of the source, but also an upgoing component. In such situations, we consider the source wavelet to also include the upgoing component of the source. Consequently, the wavelet with which we deconvolve the reflection response at the surface is no longer that of a monopole source but of a dipole source.

Although we show 1D examples, all equations are multidimensional. In 2D or 3D media, a smooth version of the slowness (1/velocity) can be used to get an estimate of the direct arriving wave from the virtual source to the surface, but the small-scale details of the velocity and density need not be known. The direct arriving wave can be obtained using finite-difference modeling of the waveforms. In 1D, a velocity model is not necessary, unless we want a depth image as in the examples we show in this paper.

We have also briefly investigate Marchenko imaging when the reflection response is corrupted with noise. In such noisy cases, the noise level in the reflection response and the Marchenko image is similar although our Green's function retrieval algorithm is nonlinear. However, further investigation is needed to properly understand the accuracy of Marchenko imaging when the reflection response is corrupted with noise.

CONCLUSION

We have extended the retrieval of the Green's function to include the presence of a free surface. This function includes primaries, internal multiples, and now also free-surface multiples. Significantly, our proposed method does not require any surface-related multiple removal of the reflection response. The resulting images of the subsurface are free of any artifacts of the free surface multiples and internal multiples; this is because Marchenko imaging is a natural way to use primaries and multiples in imaging.

APPENDIX A

GREEN'S FUNCTION RETRIEVAL IN THE PRESENCE OF THE FREE SURFACE

We discuss our adaptation of the method of Wapenaar et al. (2013b) to account for the free-surface reflections. The focusing functions are the wavefields that focus, in time and space, at a point in the medium or at the surface (Figure 2a and 2b). These focusing functions exist in the reference medium, which is homogeneous above the depth level ∂D_0 and reflection free below ∂D_i.

The reciprocity theorems for one-way (up- and downgoing) wavefields are derived by Wapenaar and Grimbergen (1996) (see equations A-3 and A-4). We use the convolution-type and correlation-type reciprocity theorems to find relationships between our up- and downgoing wavefields. As discussed by Wapenaar et al. (2014), we obtain a relationship between the focusing functions f_1 and f_2 by using their respective up- and downgoing waves at each depth level ∂D_0 and ∂D_i with the convolution reciprocity theorem

$$f_1^+(\mathbf{x_0''}, \mathbf{x_i'}, \omega) = f_2^-(\mathbf{x_i'}, \mathbf{x_0''}, \omega), \qquad (A\text{-}1)$$

and correlation reciprocity theorem

$$-f_1^-(\mathbf{x_0''}, \mathbf{x_i'}, \omega)^* = f_2^+(\mathbf{x_i'}, \mathbf{x_0''}, \omega). \qquad (A\text{-}2)$$

Our actual inhomogeneous model with a free surface above ∂D_0 is shown in Figure 3. As opposed to the model in Wapenaar et al. (2013a), which does not have a free surface, we consider the reflections from the free surface for a downgoing source similar to the work of Wapenaar et al. (2004). In Figure 3, we describe the wavefield in its up- and downgoing components. The downward-propagating component of the wavefield (Green's function) at ∂D_0 is $G^+(\mathbf{x_0}, \mathbf{x_0''}, \omega) = \delta(\mathbf{x_H} - \mathbf{x_H''}) + rR(\mathbf{x_0}, \mathbf{x_0''}, \omega)$, which includes (in the right side) the downward-going impulsive source and the reflection from the free surface. The downgoing source $\delta(\mathbf{x_H} - \mathbf{x_H''})$ is a 2D Dirac delta, where $\mathbf{x_H''}$ is the lateral position of the focal point of f_2.

Note G^+ is the component of the Green's function that is propagating downward at $\mathbf{x_0}$ for a downward radiating source at $\mathbf{x_0''}$. In the case without the free surface, there are no reflections from the free surface; hence, $G_0^+(\mathbf{x_0}, \mathbf{x_0''}, \omega) = \delta(\mathbf{x_H} - \mathbf{x_H''})$ because $r = 0$. The upward-going propagating part of the Green's function G^- at ∂D_0 is the reflection response $R(\mathbf{x_0}, \mathbf{x_0''}, \omega)$. We consider the up- and downgoing components of the Green's function at ∂D_i. The downgoing component is $G^+(\mathbf{x_i}, \mathbf{x_0''}, \omega)$, whereas the upgoing component is $G^-(\mathbf{x_i}, \mathbf{x_0''}, \omega)$ (G^+ and G^-, respectively, Figure). We use the convolution and correlation reciprocity theorems to find relationships for the one-way wavefields of f_1 as shown in Figure 2a,

and the one-way wavefields of the Green's function in the actual medium are shown in Figure 3:

$$
G^-(\mathbf{x_i'}, \mathbf{x_0''}, \omega) = \int_{\partial D_0} [f_1^+(\mathbf{x_0}, \mathbf{x_i'}, \omega) R(\mathbf{x_0}, \mathbf{x_0''}, \omega) \\
- r f_1^-(\mathbf{x_0}, \mathbf{x_i'}, \omega) R(\mathbf{x_0}, \mathbf{x_0''}, \omega)] d\mathbf{x} \\
- f_1^-(\mathbf{x_0''}, \mathbf{x_i'}, \omega), \tag{A-3}
$$

and

$$
G^+(\mathbf{x_i'}, \mathbf{x_0''}, \omega) = - \int_{\partial D_0} [f_1^-(\mathbf{x_0}, \mathbf{x_i'}, \omega)^* R(\mathbf{x_0}, \mathbf{x_0''}, \omega) \\
- r f_1^+(\mathbf{x_0}, \mathbf{x_i'}, \omega)^* R(\mathbf{x_0}, \mathbf{x_0''}, \omega)] d\mathbf{x} \\
+ f_1^+(\mathbf{x_0''}, \mathbf{x_i'}, \omega)^*. \tag{A-4}
$$

Equations A-3 and A-4 are similar to the relation for the up- and downgoing Green's function in Wapenaar et al. (2014); however, equations A-3 and A-4 also account for the reflected waves from the free surface. These free-surface reflections are the expressions in equations A-3 and A-4 that are multiplied by r. The two-way Green's function is obtained by adding equations A-3 and A-4, as well as using equations 2, 3, A-1, and A-2:

$$
G(\mathbf{x_i'}, \mathbf{x_0''}, \omega) = f_2(\mathbf{x_i'}, \mathbf{x_0''}, \omega)^* \\
+ \int_{\partial D_0} f_2(\mathbf{x_i'}, \mathbf{x_0}, \omega) R(\mathbf{x_0}, \mathbf{x_0''}, \omega) d\mathbf{x_0} \\
+ r \int_{\partial D_0} f_2(\mathbf{x_i'}, \mathbf{x_0}, \omega)^* R(\mathbf{x_0}, \mathbf{x_0''}, \omega) d\mathbf{x_0}. \tag{A-5}
$$

We consider equation A-5, in time, for the interval $t < t_d(\mathbf{x_i'}, \mathbf{x_0''})$, where t_d is the traveltime for the first arrival of G. No waves arrive before $t_d(\mathbf{x_i'}, \mathbf{x_0''})$ because t_d is the time for the first-arriving event. Therefore, $G(\mathbf{x_i'}, \mathbf{x_0''}, \omega)$ vanishes for $t < t_d(\mathbf{x_i'}, \mathbf{x_0''})$, and as a result,

$$
0 = f_2(\mathbf{x_i'}, \mathbf{x_0''}, -t) \\
+ \int_{\partial D_0} d\mathbf{x_0} \int_{-\infty}^{t} f_2(\mathbf{x_i'}, \mathbf{x_0}, t') R(\mathbf{x_0}, \mathbf{x_0''}, t - t') dt' \\
+ r \int_{\partial D_0} d\mathbf{x_0} \int_{-t}^{\infty} f_2(\mathbf{x_i'}, \mathbf{x_0}, t') R(\mathbf{x_0}, \mathbf{x_0''}, t + t') dt'. \tag{A-6}
$$

We use the same ansatz for f_2 as Wapenaar et al. (2013a) because we are using the same reference medium, i.e., the model where the focusing functions exist. The ansatz is given by

$$
f_2(\mathbf{x_i}, \mathbf{x_0''}, t) = [T_d(\mathbf{x_i}, \mathbf{x_0''}, t)]^{inv} + M(\mathbf{x_i}, \mathbf{x_0''}, t), \tag{A-7}
$$

where $[T_d(\mathbf{x_i}, \mathbf{x_0''}, t)]^{inv}$, defined as the inverse of the direct arrival of the transmission response, is the first-arriving event of $f_2(\mathbf{x_i}, \mathbf{x_0''}, t)$ and $M(\mathbf{x_i}, \mathbf{x_0''}, t)$ is the scattering coda of f_2 following the first arrival as shown by Wapenaar et al. (2013a). The substitution of expression A-7 in equation A-6 yields

$$
0 = M(\mathbf{x_i'}, \mathbf{x_0''}, -t) \\
+ \int_{\partial D_0} d\mathbf{x_0} \int_{-\infty}^{-t_d^\epsilon(\mathbf{x_i'}, \mathbf{x_0})} [T_d(\mathbf{x_i'}, \mathbf{x_0}, t')]^{inv} R(\mathbf{x_0}, \mathbf{x_0''}, t - t') dt' \\
+ \int_{\partial D_0} d\mathbf{x_0} \int_{-t_d^\epsilon(\mathbf{x_i'}, \mathbf{x_0})}^{t} M(\mathbf{x_i'}, \mathbf{x_0}, t') R(\mathbf{x_0}, \mathbf{x_0''}, t - t') dt' \\
+ r \int_{\partial D_0} d\mathbf{x_0} \int_{-t_d^\epsilon(\mathbf{x_i'}, \mathbf{x_0})}^{\infty} M(\mathbf{x_i'}, \mathbf{x_0}, t') R(\mathbf{x_0}, \mathbf{x_0''}, t + t') dt' \\
+ r \int_{\partial D_0} d\mathbf{x_0} \int_{-t}^{-t_d^\epsilon(\mathbf{x_i'}, \mathbf{x_0})} [T_d(\mathbf{x_i'}, \mathbf{x_0}, t')]^{inv} R(\mathbf{x_0}, \mathbf{x_0''}, t + t') dt', \tag{A-8}
$$

for $t < t_d(\mathbf{x_i'}, \mathbf{x_0''})$ with $t_d^\epsilon(\mathbf{x_i'}, \mathbf{x_0''}) = t_d(\mathbf{x_i'}, \mathbf{x_0''}) - \epsilon$, where ϵ is a small positive constant to include the direct arrival in the integral. Equation A-8 is a Fredholm integral of the second kind and can be solved iteratively as follows:

$$
M_k(\mathbf{x_i'}, \mathbf{x_0''}, -t) \\
= M_0(\mathbf{x_i'}, \mathbf{x_0''}, -t) \\
- \int_{\partial D_0} d\mathbf{x_0} \int_{-t_d^\epsilon(\mathbf{x_i'}, \mathbf{x_0})}^{\infty} M_{k-1}(\mathbf{x_i'}, \mathbf{x_0}, t') R(\mathbf{x_0}, \mathbf{x_0''}, t - t') dt' \\
- r \int_{\partial D_0} d\mathbf{x_0} \int_{-t_d^\epsilon(\mathbf{x_i'}, \mathbf{x_0})}^{\infty} M_{k-1}(\mathbf{x_i'}, \mathbf{x_0}, t') R(\mathbf{x_0}, \mathbf{x_0''}, t + t') dt', \tag{A-9}
$$

where

$$
M_0(\mathbf{x_i'}, \mathbf{x_0''}, -t) \\
= - \int_{\partial D_0} d\mathbf{x_0} \int_{-\infty}^{-t_d^\epsilon(\mathbf{x_i'}, \mathbf{x_0})} [T_d(\mathbf{x_i'}, \mathbf{x_0}, t')]^{inv} R(\mathbf{x_0}, \mathbf{x_0''}, t - t') dt' \\
- r \int_{\partial D_0} d\mathbf{x_0} \int_{-t}^{-t_d^\epsilon(\mathbf{x_i'}, \mathbf{x_0})} [T_d(\mathbf{x_i'}, \mathbf{x_0}, t')]^{inv} R(\mathbf{x_0}, \mathbf{x_0''}, t + t') dt', \tag{A-10}
$$

for $t < t_d(\mathbf{x_i'}, \mathbf{x_0''})$ and $M_k(\mathbf{x_i'}, \mathbf{x_0''}, -t) = 0$ for $t \geq t_d(\mathbf{x_i'}, \mathbf{x_0''})$. In contrast to the algorithm of Wapenaar et al. (2013a), we use R instead of R_0, and we also include the reflection from the free surface (the last term in equation A-9). After convergence, we substitute the coda M into equation A-7 to yield the focusing function f_2. The f_2 solution is then used in equation A-5 to obtain the two-way Green's function.

REFERENCES

Amundsen, L., 2001, Elimination of free-surface related multiples without need of the source wavelet: Geophysics, **66**, 327–341, doi: 10.1190/1.1444912.

Bakulin, A., and R. Calvert, 2006, The virtual source method: Theory and case study: Geophysics, **71**, no. 4, SI139–SI150, doi: 10.1190/1.2216190.

Behura, J., K. Wapenaar, and R. Snieder, 2012, Newton-Marchenko-Rose imaging: 82nd Annual International Meeting, SEG, Expanded Abstracts, doi: 10.1190/segam2012-1531.1.

Broggini, F., and R. Snieder, 2012, Connection of scattering principles: A visual and mathematical tour: European Journal of Physics, **33**, 593–613, doi: 10.1088/0143-0807/33/3/593.

Broggini, F., R. Snieder, and K. Wapenaar, 2012, Focusing the wavefield inside an unknown 1D medium: Beyond seismic interferometry: Geophysics, **77**, no. 5, A25–A28, doi: 10.1190/geo2012-0060.1.

Broggini, F., R. Snieder, K. Wapenaar, and J. Behura, 2014, Wavefield autofocusing and imaging with multidimensional deconvolution: Numerical examples for reflection data with internal multiples: Geophysics, **79**, no. 3, WA107–WA115, doi: 10.1190/geo2013-0307.1.

Claerbout, J., 1971, Toward a unified theory of reflector mapping: Geophysics, **36**, 467–481, doi: 10.1190/1.1440185.

Claerbout, J., 1985, Imaging the earths interior: Blackwell Scientific Publications.

Jiang, Z., J. Sheng, J. Yu, G. Schuster, and B. Hornby, 2007, Migration methods for imaging different-order multiples: Geophysical Prospecting, **55**, 1–19, doi: 10.1111/j.1365-2478.2006.00598.x.

Muijs, R., J. O. A. Robertsson, and K. Holliger, 2007a, Prestack depth migration of primary and surface-related multiple reflections. Part I: Imaging: Geophysics, **72**, no. 2, S59–S69, doi: 10.1190/1.2422796.

Muijs, R., J. O. A. Robertsson, and K. Holliger, 2007b, Prestack depth migration of primary and surface-related multiple reflections. Part II: Identification and removal of residual multiples: Geophysics, **72**, no. 2, S71–S76, doi: 10.1190/1.2424544.

Rose, J., 2002a, Single-sided autofocusing of sound in layered materials: Inverse Problems, **18**, 1923–1934, doi: 10.1088/0266-5611/18/6/329.

Rose, J., 2002b, Time reversal, focusing and exact inverse scattering, *in* M. Fink, W. A.. Kuperman, J.-P. Montagner, and A. Tourin, eds., Imaging of complex media with acoustic and seismic waves: Springer, 97–106.

Schuster, G. T., Z. Jiang, and J. Yu, 2003, Imaging the most bounce out of multiples: 65th Annual International Meeting and Conference, EAGE, Extended Abstracts, P4.

Slob, E., K. Wapenaar, F. Broggini, and R. Snieder, 2014, Seismic reflector imaging using internal multiples with Marchenko-type equations: Geophysics, **79**, no. 2, S63–S76, doi: 10.1190/geo2013-0095.1.

Van der Neut, J., J. Thorbecke, K. Mehta, E. Slob, and K. Wapenaar, 2011, Controlled-source interferometric redatuming by crosscorrelation and multidimensional deconvolution in elastic media: Geophysics, **76**, no. 4, SA63–SA76, doi: 10.1190/1.3580633.

Verschuur, D., A. Berkhout, and C. Wapenaar, 1992, Adaptive surface-related multiple elimination: Geophysics, **57**, 1166–1177, doi: 10.1190/1.1443330.

Wapenaar, C. P. A., and J. L. T. Grimbergen, 1996, Reciprocity theorems for one-way wavefields: Geophysical Journal International, **127**, 169–177, doi: 10.1111/j.1365-246X.1996.tb01542.x.

Wapenaar, K., F. Broggini, E. Slob, and R. Snieder, 2013a, Three-dimensional single-sided Marchenko inverse scattering, data-driven focusing, Green's function retrieval, and their mutual relations: Physical Review Letters, **110**, 084301, doi: 10.1103/PhysRevLett.110.084301.

Wapenaar, K., E. Slob, J. van der Neut, J. Thorbecke, F. Broggini, and R. Snieder, 2013b, Three-dimensional Marchenko equation for Green's function retrieval beyond seismic interferometry: 83rd Annual International Meeting, SEG, Expanded Abstracts, 4573–4578.

Wapenaar, K., , F. Broggini, and R. Sniederet al., 2011, A proposal for model-independent 3D wave field reconstruction from reflection data: 81st Annual International Meeting, SEG, Expanded Abstracts, 3788–3792.

Wapenaar, K., and J. Fokkema, 2006, Green's function representations for seismic interferometry: Geophysics, **71**, no. 4, SI33–SI46, doi: 10.1190/1.2213955.

Wapenaar, K., J. Fokkema, M. Dillen, and P. Scherpenhuijsen, 2000, One-way acoustic reciprocity and its applications in multiple elimination and time-lapse seismics: 80th Annual International Meeting, SEG, Expanded Abstracts, 2377–2380.

Wapenaar, K., J. Thorbecke, and D. Draganov, 2004, Relations between reflection and transmission responses of three-dimensional inhomogeneous media: Geophysical Journal International, **156**, 179–194, doi: 10.1111/j.1365-246X.2003.02152.x.

Wapenaar, K., J. Thorbecke, J. van der Neut, F. Broggini, E. Slob, and R. Snieder, 2014, Green's function retrieval from reflection data, in absence of a receiver at the virtual source position: Journal of the Acoustical Society of America, **135**, 2847–2861, doi: 10.1121/1.4869083.

Weglein, A., and W. Dragoset, 2007, Multiple attenuation: SEG 23, *of* Geophysics Reprint Series, 482.